Nuclear Engineering and Design 435 (2025) 113920

Contents lists available at ScienceDirect

Nuclear Engineering and Design

journal homepage: www.elsevier.com/locate/nucengdes

Gen-IV pool reactors: Validation of sloshing CFD modelling and behavior under large seismic events☆

Vincent Moreau *, Manuela Profir

CRS4 Pula, Sardinia, Italy

ARTICLE INFO

Keywords:
ALFRED
PASCAL
FALCON
CFD
Sloshing
VoF

ABSTRACT

This paper addresses one aspect of the safety of compact lead-cooled pool fast reactors. Under a seismic event, there is concern that the surface sloshing could compromise the integrity of some structures or components. We investigate this issue by means of computational modelling and simulation using the STAR-CCM + commercial software.

In the first part, we simulate a partially filled vertical cylinder under harmonic forcing and quantitatively validate the modelling by comparison with experimental data of the free-surface height at different locations. Specifically, we capture with a very high precision a behavioral transition of the amplitude-frequency map near resonance.

In the second part, the modelling is applied to a fast reactor mock-up in water. It is validated again by comparison with experimental data under harmonic forcing. The numerical mock-up is then subjected to four seismic events of increasing intensity. The free-surface height and the forces applied to the mock-up vessel are monitored.

It is found that the forces applied to the vessel are strongly dominated by the highest frequency of the seismic acceleration. By applying a high filter cut at 1 Hz, the peak force is reduced by one order of magnitude but remains strongly related to the damped acceleration signal. Even then, sloshing forcing effects are observed but remain marginal.

1. Introduction

In the framework of the Generation IV (GEN IV) innovative nuclear systems, the Generation IV International Forum (GIF)[1] recognizes the Lead-cooled Fast Reactors (LFRs) as one of the most promising concepts. Several European Atomic Energy (EURATOM) projects focus on Heavy Liquid Metal (HLM) technology, materials investigations, modelling, simulations and licensing for LFRs. The Fostering ALfred CONstruction (FALCON) international consortium, led by ENEA, Ansaldo Nucleare and RATEN-ICN, is dedicated to the construction and operation of the Advanced Lead-cooled Fast Reactor European Demonstrator (ALFRED) in Romania, demonstrating the LFR technology viability (Cioli Puviani et al., 2024).

In the Horizon 2020 EURATOM "Proof of Augmented Safety Conditions in Advanced Liquid-metal-cooled systems" (PASCAL[2]) project, one of the objectives is to understand whether there is a sloshing issue with reactors such as ALFRED under a strong seismic event. A specific task, as written in the proposal, is "[t]o further enhance the modelling and computational readiness level of sloshing dynamics in compact liquid–metal filled pools and to retrieve the expected impact forces and dislocations on the involved components for a reference system (e.g. ALFRED)."

The task is coordinated by the Von Karman Institute (VKI). VKI mainly focuses on the experimental part using its SHAKESPEARE seismic table[3] while CRS4 concentrates on the CFD simulation and modelling part using the commercial STAR-CCM + software on its HPC

☆ This article is part of a special issue entitled: 'LFR' published in Nuclear Engineering and Design.

* Corresponding author.
E-mail address: moreau@crs4.it (V. Moreau).

[1] https://www.gen-4.org.

[2] Grant agreement number 945,341.

[3] https://www.vki.ac.be/index.php/facilities-other-menu-148/safety-facilities/304-research-and-consulting/facilities/seismic-facilities/691-shakespeare.

https://doi.org/10.1016/j.nucengdes.2025.113920
Received 5 December 2024; Received in revised form 22 January 2025; Accepted 13 February 2025
Available online 20 February 2025

cluster.[4] The jointly developed experimental design is based on literature review, past experience, material constraints and additional analyses.

The two research institutions already demonstrated some related background: in (Myrillas et al., 2015), the SHAKESPEARE table was used to investigate sloshing in a 6 cm radius cylinder, comparing water and mercury behavior under the same forcing; in (Moreau et al., 2019), a CFD model of the MYRRHA[5] primary coolant loop, comprising several interconnected free-surfaces changing level during incidental transients, has been presented. The current work is strongly conditioned by and benefits from this past experience.

The progress of the work is documented by several Technical Review Meetings, workshop and conference presentations publicly available on the authors institutional websites.[6] It is also documented by two public deliverables of the PASCAL project authored by CRS4 (Moreau et al., 2023; Moreau and Profir, 2024) and one authored by VKI (Frandsen et al., 2024). This paper attempts to summarize these documents, presenting the most relevant results and findings of this task, from the CRS4 numerical modelling and simulation point of view.

A thorough description of the experimental setup corresponding to the simulations presented here can be found in (Frandsen et al., 2024; Muller et al., 2023) and (Grasso, 2024).

Sloshing is a very broad subject which can easily become dispersive. A good introduction to the subject can be found in (Royon-Lebeaud, 2005) in French or in (Myrillas et al., 2015) and (Grasso, 2024). For our engineering-oriented approach, it is useful to know that a linear theory has been developed for partially filled vertical cylinders which gives the sloshing resonance frequencies. Besides, an extensive experimental work on partially filled vertical cylinders under harmonic forcing is documented in the Royon-Lebeaud PhD thesis (Royon-Lebeaud, 2005) and a related article (Hopfinger and Baumbach, 2009). Specifically, experimental asymptotic sloshing heights and a stability map of the first natural frequency mode are provided.

From the numerical point of view, at the beginning of the project, we could find no literature on the validation of sloshing simulations in a partially filled vertical cylinder. However, we were able to find a mention of unreferenced successful simulations (Sharma et al., 2019) but these were characterized as costly and extremely user dependent. In fact, our experience is that CFD simulation of sloshing is relatively straightforward and qualitatively meaningful. The main difficulty is to move from qualitative to quantitative simulations. And for this, we focused on validation exclusively through comparison with controlled experimental data, in order to establish a first preliminary proof of feasibility.

The first experimental campaign is based on a very simple geometry, a partially filled vertical cylinder under harmonic forcing with different amplitudes and frequencies. It aims at gaining confidence with the experimental setup, the acquisition, elaboration and transfer of data, the numerical modelling, setting and simulation, hopefully concluding with the numerical model validation by comparison with the experimental data. For the first experimental campaign, only kinematic aspects are investigated.

The second experimental campaign is based on a more complex geometry with features relevant of the ALFRED design with more articulated flow paths. We will refer to the new experimental model and its numerical counterpart as the ALFRED mock-up. Moreover, investigations on dynamics aspects are also considered. The numerical framework developed for the first experimental campaign is re-validated and is improved and extended to cope with the system dynamics. The modelling is then applied to configurations relevant of four documented seismic events of increasing intensity. Each one of them brings new insights and technical considerations. The last two investigated events involve displacements that are too large to be performed by the seismic table at the mock-up scale.

[4] https://www.crs4.it/services/high-performance-computing/.

[5] https://myrrha.be/en.

[6] https://www.crs4.it/peopledetails/50/vincent-moreau/ and https://www.crs4.it/peopledetails/269/maria-manuela-profir/.

2. Sloshing CFD validation

2.1. Test case determination

The CFD modelling and simulation must be validated by comparison with fully controlled experimental data provided by VKI in the framework of the PASCAL European project (Frandsen et al., 2024). We consider a vertical cylinder partially filled with water. The cylinder is subjected to harmonic forcing with different amplitudes and frequencies. The main data provided is the free-surface height in coincidence with four cardinal vertical capacity probes close to the cylinder boundary.

In addition to its simplicity, this configuration has many advantages. As an alternative to mercury, water is widely available and do not require strict safety measures. Water is lighter than mercury, so that at weight parity a larger cylinder can be used. In turn, surface tension effects decrease and, at parity of absolute precision, the relative accuracy of measurements improves. Plexiglas cylinder and water are transparent, allowing to observe the production of bubbles. A vertical cylinder allows an easy fitting of vertical probes from the top to monitor the free-surface height. Finally, for a partially filled vertical cylinder, the resonance frequency is known and is independent of the specific weight, which means that water or mercury can equally represent the lead.

The cylinder is filled with water up to a height of 1.5 radius, value for which the linear theory predicts a negligible bottom effect on the resonance frequency.

The cylinder diameter can now be determined considering that is must be the largest possible for measurement accuracy and must be easily purchasable on the market. The filling depth must be such that upon scaling, the Royon-Lebeaud (Muller et al., 2023; Grasso, 2024) experimental campaign can be replicated with the SHAKESPEARE table, limited to a maximum displacement amplitude of 4.5 cm.

The cylinder diameter is therefore $\sim$ 60 cm, almost four times the Royon-Lebeaud one. In fact, our initial objective is to reproduce their work. The cylinder is filled with water for up to 45 cm, that is up to 1.5 times its radius from its flat bottom.

In order to compare with Royon-Lebeaud's work and to extrapolate to ALFRED, we need to make some considerations on the dimensional analysis which is discussed more deeply in (Myrillas et al., 2015). First of all, we want to only consider kinematic similarities. This means that only length and time are involved. We definitively need the geometrical similarity and so our leading parameter is a reference length and we opt for the cylinder radius. Sloshing is primarily characterized by the resonance frequency. For sufficiently large cylinders, the natural frequency scales with the inverse square root of the radius (Myrillas et al., 2015). This means that when we have to extrapolate to ALFRED, time scales with the radius square root and the acceleration is an invariant of the scaling. In fact, acceleration must be invariant because ALFRED and its mock-up are affected by the same gravitational force.

2.2. Reference test case for calibration

The reference test case chosen to calibrate the numerical setting is the following:

- Flow initially at rest
- Forcing frequency: 92 % of the natural frequency $f_0 = 1.236$ Hz.
- Asymptotic amplitude: A = 4 mm (1.33 % of radius).
- Initial amplitude linear ramp over 4 periods.

In order to define a meaningful Reynolds number, the velocity must

be representative of the fluid velocity which is a priori unknown under harmonic forcing. Far away from resonance, a sound educated guess is to use the maximum forcing velocity. Closer to resonance, but still in the planar asymmetric regime, this choice loses meaning because the forcing displacement becomes much lower than the fluid elevation. For the chosen test case, the maximum elevation at the probe is about 100 mm after 8 s and still above h = 60 mm at the next 5 beats maximum leading to a reference velocity of $h*2\pi*0.92*f_0 = 0.43$ m/s. With the water viscosity at 10^{-6} m^2/s, and taking the cylinder radius as characteristic length, the Reynolds number reaches about 130,000. This is why we clearly expect a turbulent regime.

2.3. Numerical setting

The numerical model is based on the Volume of Fluid (VoF) paradigm in which two phases, water and air, share the same velocity and pressure field but are characterized by their volume fraction transport equation. The displacement is explicitly set by using the rigid body mesh moving feature, so that the model is considered from a fixed inertial (except for gravity) reference frame. The alternative would have been to add a force term into the momentum equation and view the model in its own reference frame. However, direct visual observation of the displacement helps to ensure that the model is given the correct input data.

It took a very long time, of trial and errors, to find a numerical setting that correctly reproduced the experimental test case (Moreau et al., 2023). Due to the current rapid evolution of CFD with regard to the two-phase flow implementation, we must acknowledge that these settings are partly software dependent and even partly software version dependent. The ones that we retain of particular relevance are given below as an indication.

- Input data: the numerical input displacement data is given analytically using the formula used to prepare the input file of the shaking table. Direct measurements of the table position suffer from signal noise and their use perturbs the simulation results.
- Mesh: trimmed and aligned to the initial free-surface.
  - o Main size: 5 mm
  - o Two levels of mesh adaption around the free surface, minimum mesh size 1.25 mm.
  - o Adaption is performed each 5 time-steps
  - o Boundary layer: 50 % of mesh size (2.5 mm), 3 layers, 1.5 ratio.
- Time-step controlled by two CFL criteria, using STAR-CCM + default values:
  - o CFL limiter on the flow velocity
  - o CFL limiter on the free-surface velocity.
- Relaxation factor on pressure increased from default 0.2 to 0.45, meaning less relaxation.
- Laminar simulation: this setting has been very difficult to accept but is the only one giving satisfying results.

The numerical equivalent of the experimental probe is obtained by restricting the free-surface derived part to a small neighborhood around the probe position and taking its mean vertical position. This is illustrated in Fig. 1.

2.4. First validation results

Validation is performed by comparing the time history of the free surface elevation at one of the probe positions. For 1D harmonic forcing in the stable part of the stability map, only one position needs to be checked as the opposite one is only shifted by half a period and the orthogonal positions are almost still.

In order to understand what has been accepted as a validation result, in Fig. 2 on the left, we show the first unfitted numerical-experimental comparison on one elevation probe. The simulation was performed

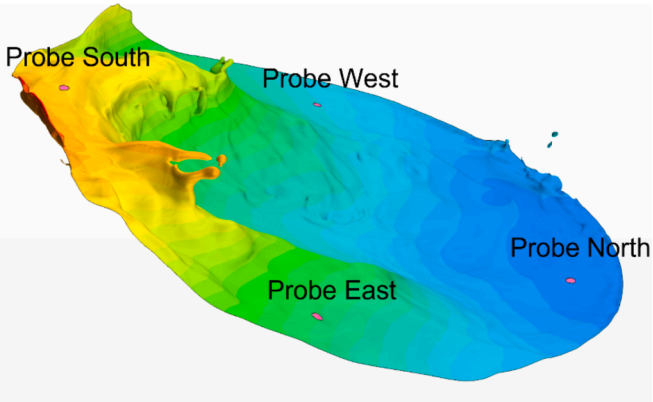

Fig. 1. Numerical probes relative to the free-surface. The height is obtained by taking its mean value over the very small pink regions just below the legends.

using the Realizable K-Epsilon Two-Layer All y + Wall Treatment with default software values. The experimental curve shows an oscillatory behavior at the forcing frequency, strongly modulated at a much lower frequency. The envelop of the curve shows a strong maximum at about twice the asymptotic value, then a strong interference-like node followed by a less intense envelop maximum and a progressive dissipation of the low frequency beat. The preliminary simulation, using a turbulence model, fails to reproduce these experimental features.

Even if not satisfactory, this preliminary simulation allows to define some criteria required for validation. A validated simulation is the one able to correctly reproduce the timing and the amplitude of the first two beats and of the first intermediate node. This has been obtained after a long optimization procedure, as shown in Fig. 2 on the right, upon applying the settings of the previous sub-section.

2.5. Validation from stability transition value

The first validation is limited to the fact that we were dealing with a simple sloshing flow. The work of Royon-Lebeaud strongly suggests that there is a transition to chaotic behavior at some point when the frequency is increased towards the resonance frequency. To our surprise, the transition frequency observed experimentally by VKI is about 2 % of the resonance frequency in advance of the Royon-Lebeaud measurement. This was totally unexpected and worried the experimentalists who questioned the experiment validity.

It turns out that the transition to chaos is numerically observed at the same value, within 0.1 %, as in the VKI experiments. This is a rare case where simulations and experiments cleave to each other. The transition is observed experimentally between 92.55 and 92.6 % of the resonance frequency, while it is found numerically between 92.4 and 92.5 %. This can be seen by looking at the activation of the north probe. In Fig. 3, we show the numerical evolution of the free-surface level at the east and north probes as we approach the frequency transition to chaos. The first beat of the east probe progressively widens and increases in peak value and from 92 % to 92.4 %, then there is a run-away at 92.5 % followed by the activation of the north probe. The experimental value of the east probe at 92.55 % is also given on Fig. 3 bottom-right, and it coincides almost perfectly with the numerical value at 92.5 % during the first 15 s.

By accurately controlling the initial phase of the forcing, we can observe the changes in the free-surface height curve as it approaches and passes the transition value. Due to the nature of the flow and its sensitivity to initial conditions, the numerical flow cannot precisely reproduce the experimental flow above the transition value. However, all the main phases of the flow, as described by Royon-Lebeaud: (i) planar rise to splashing, (ii) swirling in one direction, (iii) stop, (iv) swirling in the other direction, (v) stop, (vi) repeat, clearly appear with the same sequence order. Three instants of the free-surface at 4 mm amplitude

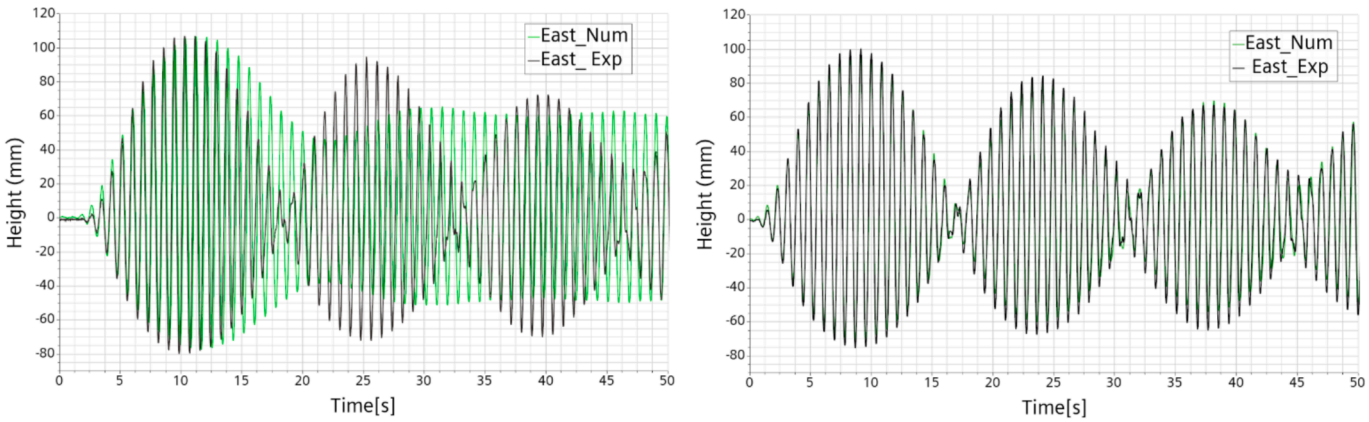

Fig. 2. Experimental/numerical comparison of the East probe free-surface level under harmonic forcing. Left, initial turbulent setting. Right, optimized laminar setting.

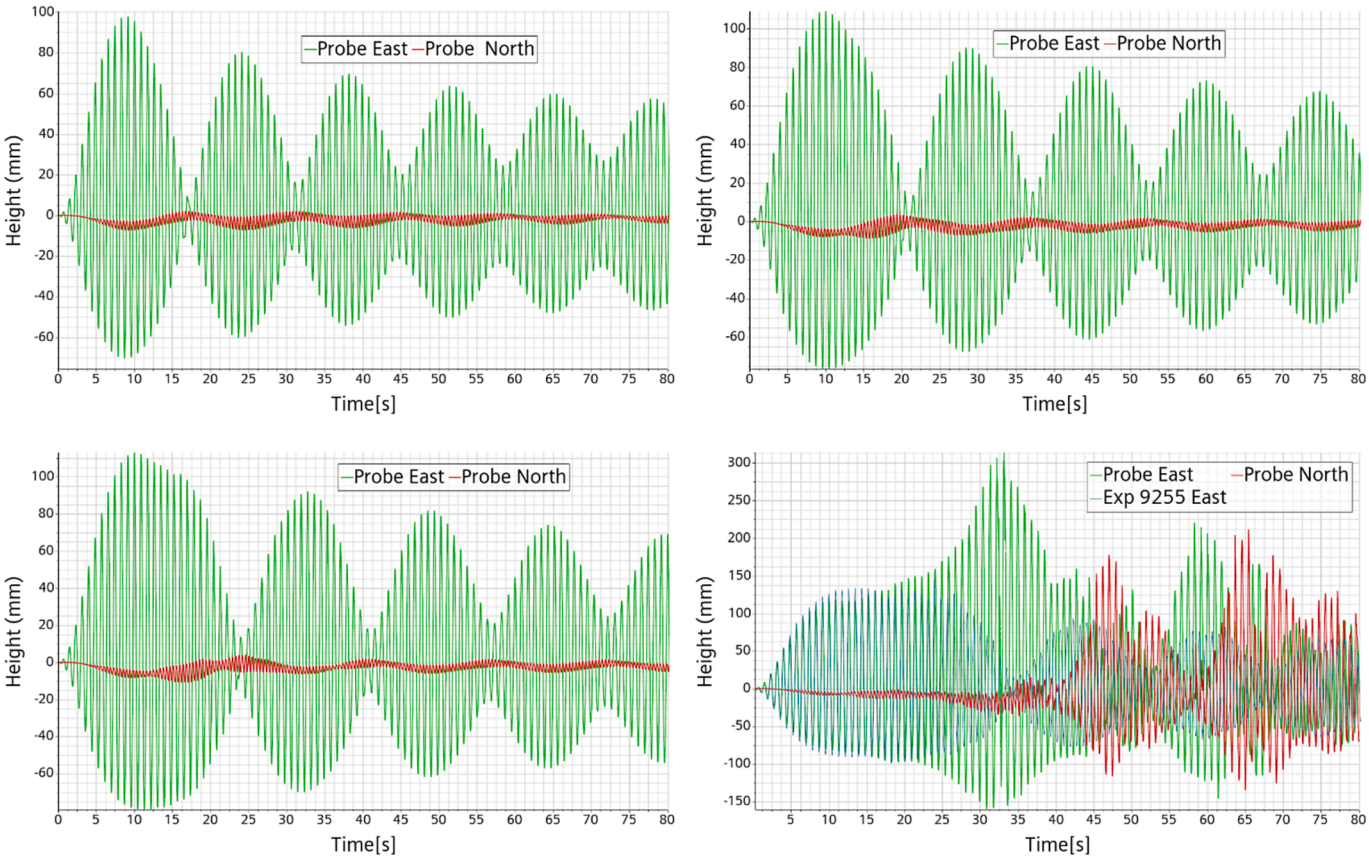

Fig. 3. Numerical transition vs. chaos. Amplitude 4 mm. Frequency 92 % (top-left), 92.3 %(top-right), 92.4 % (bottom-left) and 92.5 % (bottom-right) with also, in blue, the East probe experimental measurements at 92.55 %.

and 92.5 % of resonance frequency are shown on Fig. 4.

The stability limit at 4 mm amplitude is reproduced very accurately by the numerical simulation. This is a very sensitive property of the flow which is correctly captured. This feature is considered as a strong validation of the numerical model.

2.6. *Extension of the stability map*

Although the numerical model is considered to be sufficiently validated, we also discovered an unexpected dependence of the stability map on the cylinder radius and decided to investigate this aspect numerically.

For a vertical cylinder filled for 1.5 its radius, all other things being equal, under a linear horizontal harmonic forcing of moderate amplitude starting smoothly, the asymptotic free-surface behavior observed exhibits three clearly differentiated modes: (i) an asymmetric planar wave aligned with the forcing, (ii) a swirling mode and (iii) a so-called chaotic behavior. The main controlling parameters are the forcing amplitude and the forcing frequency, both normalized respectively by the cylinder radius and the resonance frequency. For the first two modes, an asymptotic wave amplitude can be defined. A stability map in the form of an amplitude-frequency diagram, such as the one shown in Fig. 5 can be drawn to summarize the observed experimental and numerical results.

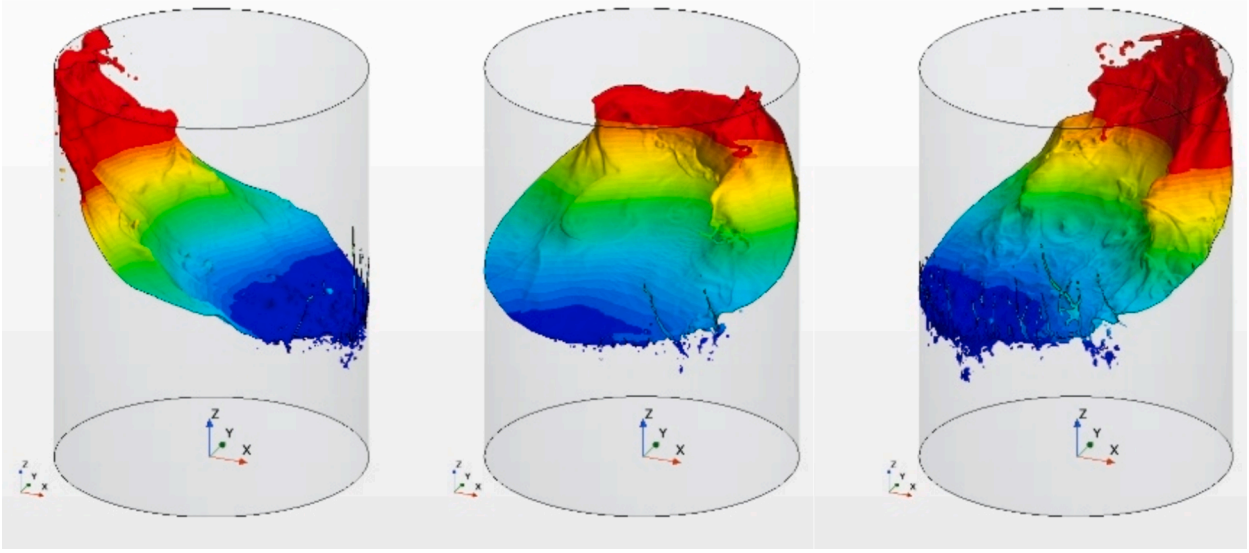

Fig. 4. Harmonic forcing, amplitude 4 mm and frequency 92.5 % of resonance. Free-surface at the first east peak amplitude, time 33.6 s (left), at the north first peak amplitude, time 47.0 s (center) and at time 63.62 s (right. Colored by height in range [-0.35; 0.60] m.

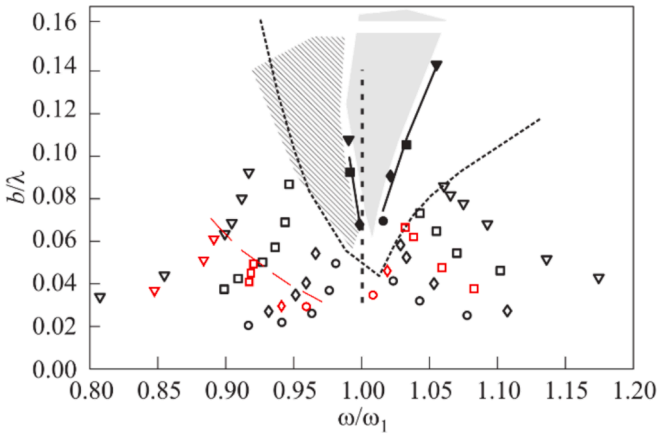

Fig. 5. Stability map from (Hopfinger and Baumbach, 2009) in black, cylinder radius r = 7.8 cm, with our simulation results added in red, cylinder radius r = 30 cm. Horizontal axis: the frequency normalized by the resonance one. Vertical axis: a normalized elevation amplitude (λ = 3.411 r). Symbols refer to cylinder radius fraction of the forcing amplitude: triangle 2.67 %, square 1.33 %, rhombus 0.67 % and circle 0.33 %. Dotted lines indicate the stability limit of the asymmetric planar wave for r = 7.8 cm. Open symbols indicate planar mode and filled ones indicate the boundaries of the swirling mode. Chaos is observed in the hatched region, extending towards left up to the red dashed line for r = 30 cm.

As already observed, the position of the bifurcation line on the stability map seems to depend on the cylinder radius. In fact, as the radius increases and, while maintaining the geometrical and frequency similarity, the Reynolds number increases and surface tension effects decrease. The increase in the Reynolds number means that there is a wider range of high frequency secondary flows. Still keeping tests cases in geometrical and frequency similarity, the decrease of surface tension effects makes droplets and bubbles appear more easily. It is therefore a posteriori not so surprising that increased small scale features can destabilize the first resonance frequency mode.

To get a better idea on the position of the transition curve with our cylinder of larger radius, we performed a series of simulations at different amplitude and frequencies, still following the Royon-Lebeaud approach. The results are superposed on the stability map as given in (Hopfinger and Baumbach, 2009) and shown in Fig. 5. For each forcing amplitude, only the simulations providing a clear planar motion asymptotic maximum elevation are indicated. Simulations with frequencies slightly closer to resonance lead to the bifurcation behavior. All the simulations are also summarized in Table 1 together with the asymptotic behavior and the asymptotic height in mm, when applicable.

Table 1
Results of the simulations performed for the 30 cm radius cylinder, depending on the forcing amplitude and the normalized frequency.

Forcing amplitude (mm)	Normalized frequency (%)	Asymptotic behavior	Asymptotic maximum height (mm)
4	92	Planar asymmetric	40
4	92.3	Planar asymmetric	45
4	92.4	Planar asymmetric	50
4	92.5	Chaotic	–
4	1.08	Planar asymmetric	35
4	1.06	Planar asymmetric	46
4	1.04	Planar asymmetric	60
4	1.03	Planar asymmetric	67
4	1.025	Swirling	–
8	85	Planar asymmetric	45
8	88	Planar asymmetric	50
8	89	Planar asymmetric	59
8	89.5	Chaotic	–
2	94	Planar asymmetric	29
2	95	Chaotic	–
2	104	Planar asymmetric	58
2	102	Planar asymmetric	47
2	101	Swirling	–
1	96	Planar asymmetric	22
1	97	Chaotic	–
1	101	Planar asymmetric	34
1	100	Chaotic	–

In particular, when entering the swirling region, the simulations would have required an unaffordable duration to observe an asymptotic height. For our larger cylinder, there is a clear extension of the chaotic region towards the lower frequencies on the left part of the map. On the right side of the map where there is a transition boundary between asymmetric planar and circular motion, something different occurs. For the same forcing amplitude, the asymmetric planar motion is more stable and the relative amplitude of the asymptotic wave is lower with the larger radius, which is also reported experimentally for the 4 mm amplitude in (Muller et al., 2023). These two effects combine to keep the stability map right transition line unchanged.

The transition from asymmetric planar to circular motion under the prescribed forcing can be quite long to appear, exceeding 100 s of physical time in some simulations, making precise bounds difficult and numerically expensive to obtain. We have attempted to find an amplitude at which the asymmetrical planar wave remains stable at the resonance frequency. Trials above 1 mm showed instability after some increase in time while reducing the amplitude. At the very low amplitude forcing of 1 mm (0.33 %), precisely at the natural frequency, the flow transition from asymmetric planar to swirling happened after 100 s. After 140 s, it develops a circulating solitary wave which grows and ends splashing on the wall. After 180 s, the surface enters a rotating multi-spilling mode. Some of the most peculiar time frames are shown in Fig. 6, while the entire animation, among others, can be downloaded here.[7] This simulation was made after the end of the experimental campaign, so we do not know if it can be reproduced experimentally.

3. ALFRED mock-up under seismic events

3.1. Mock-up geometry and mesh

The numerical setting is applied to an ALFRED mock-up, designed, built and operated in water by VKI. The mock-up is only partially representative of the ALFRED design. It contains however several relevant features. The Pump Pipes (PP), the Decay Heat Removal (DHR) components and the Steam Generators (SG) are represented in some way. These components cross a hollow diaphragm plate. With this configuration, several possible hydraulic connections allow non trivial flow paths.

The CAD file was provided by VKI to CRS4 as basis for the CFD geometry. The CFD geometry is a somewhat simplified version of the CAD geometry. Some, but not all, very small-scale features such as screw heads are omitted.

The CFD geometry is illustrated in Fig. 7 and in Fig. 9 left. The main features of the mock-up are as follows:

- Vertical cylinder of radius 19.8 cm and height 39.5 cm
- Diaphragm horizontal plate 20 cm from the top
- Initially filled up to 8.84 cm above the diaphragm
- Tori-spherical bottom
- 3PPs, 3 DHRs and 3 SGs evenly spaced in circle at 40 degrees intervals.

Unfortunately, from the CFD point of view, some very small-scale features could not be ignored. In particular, there are 2 mm wide annular bypasses between the diaphragm and the PP and SG components. The gap serves to accommodate screw heads and as a margin for the components insertion. The bypass flow there could at first glance be considered negligible but in fact can be quite relevant. The pump shaft would-be hydraulic resistance is represented by a resisting plate drilled with many small holes. The drilled plate cannot be numerically represented by a resistive porous medium because there is too much uncertainty on its resistance factors. Since we need a direct validation from experimental data, these small-scale features had to be taken into account in the CFD geometry and properly discretized. As a result, a lot of effort had to be devoted to the correct representation of the bypass flows which is not the core subject of this work. The mesh before applying the adaptive remeshing is composed of 2.16 million control volumes and is illustrated in Fig. 8.

3.2. Mock-up CFD model validation

The experimental mock-up is equipped with three vertical level probes located outside the PPs, see Fig. 9 left. Data from an experimental campaign on the mock-up have been provided by VKI. Three test cases of harmonic linear forcing have been reproduced with the CFD code, using the methodology previously presented, see Fig. 9 right, and the results have been compared. The agreement is good but not as excellent as it was with the simple cylinder. An example is given in Fig. 10. There are many possible sources of discrepancies and uncertainties. The oscillation small progressive shift between numerical and experimental is not always in the same direction, making it difficult to identify its origin. The local maximum height difference also changes sign. Overall, the global behavior is very much similar. The small but noticeable discrepancies could be due to small geometrical differences, such as the numerical simplifications or the difficulty of precisely centering the component insertion in the diaphragm.

3.3. Setting upgrade to dynamics effects

The objective of this exercise is to qualify the numerical model for seismic events, quantifying the forces on the structures and components of the mock-up. The force exerted by the fluid can be measured in any direction by integrating the force intensity applied to any surface. However, it is very easy to measure critically erroneous values resulting from numerical and physical considerations that were previously irrelevant with regard to the flow characteristics.

The force exerted on a given surface is mainly due to the pressure exerted by the fluid. This pressure reacts strongly and instantaneously to oppose the surface acceleration. It is therefore very important that the surface acceleration, resulting from the imposed displacement, is correctly set. The displacement can be given by an input table at a given sampling interval which for our application is 0.01 s. By default, the code linearly interpolates the position between two consecutive samples. This means that, between two samples, the velocity is constant and therefore the acceleration is zero. The acceleration is all concentrated at the time steps that cover a sample time. This is not a problem when the time step is much larger than the sampling interval. But, in our case, the time-step is CFL controlled and is generally much smaller than the sampling interval. This again results in periodic unphysical pressure spikes. The remedy is to have the code perform a higher order interpolation method. In STAR-CCM+, a cubic interpolation can be used. It first calculates a slope at the sampling points, then passes a third order polynomial between each two consecutive points, forcing equality of position and slope at the end points. In this way, the acceleration is continuous between two points and with a finite jump when crossing a point.

Seismic acceleration signals are naturally highly variable. It is not surprising that the forces in the simulation are also highly variable. However, we found that the peak forces were reduced by up to one order of magnitude simply by applying cubic regularization to the input data, as illustrated on Fig. 11 by looking at the scales involved. Note that displacement data tables are created by numerically integrating the acceleration table twice.

Another important source of spurious forces is related to the detrimental interaction between the adaptive mesh technique and the second order time scheme. Initially, tests were carried out both with first order and second order time schemes with no indication as to which was better. Therefore, second order was chosen because it was less likely to

[7] https://publications.crs4.it/pubdocs/2024/MP24c/.

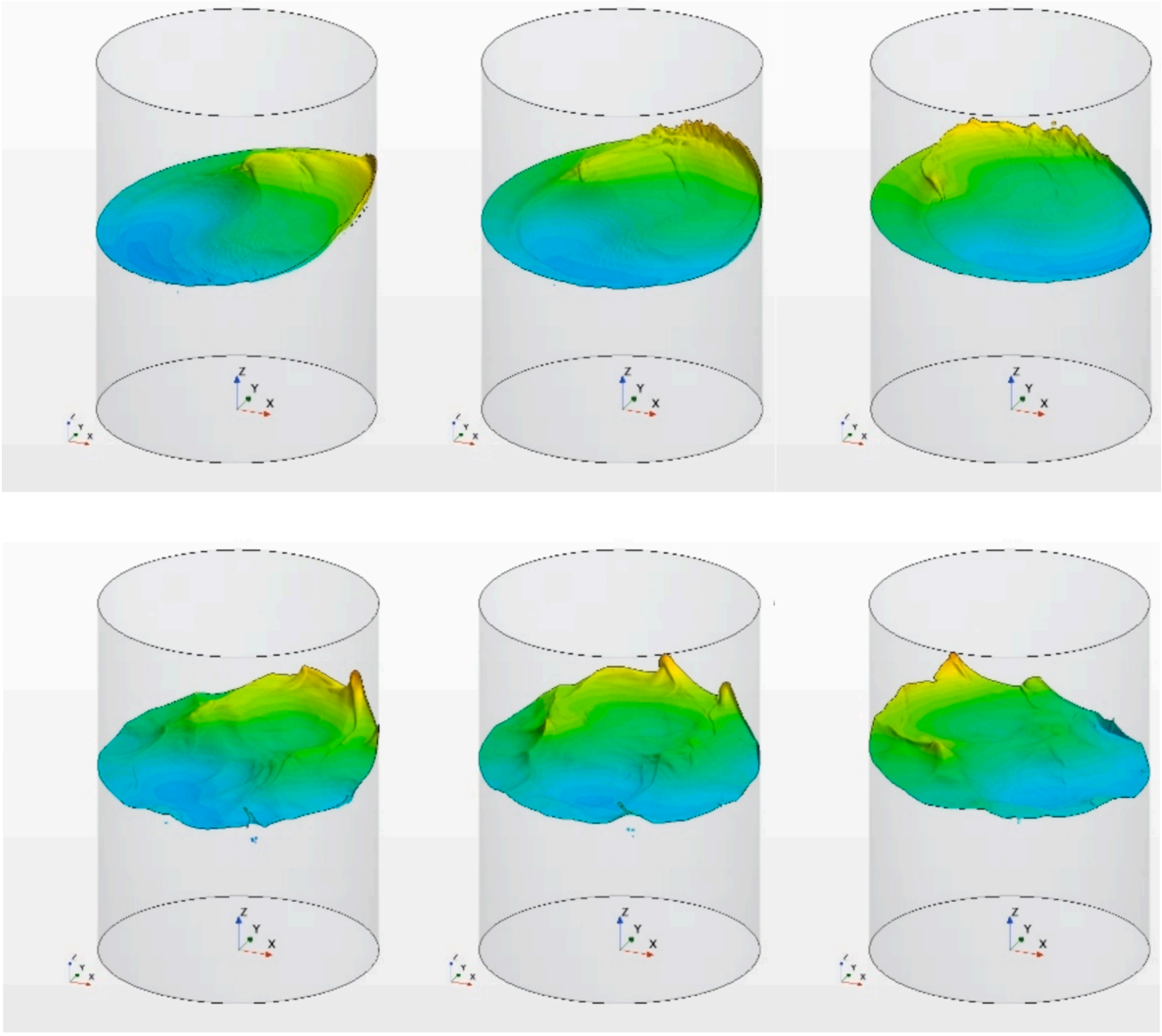

Fig. 6. Linear harmonic forcing at resonance and amplitude 1 mm. Top: development of a solitary ware and splashing of its trail at times 147.9 s (left), 148.0 s (center) and 148.1 s (right). Bottom: rapid succession of local spilling at the wall at time 215.80 s (left), 215.88 s (center) and 215.98 s (right). Colored by height in range [-0.35; 0.60] m.

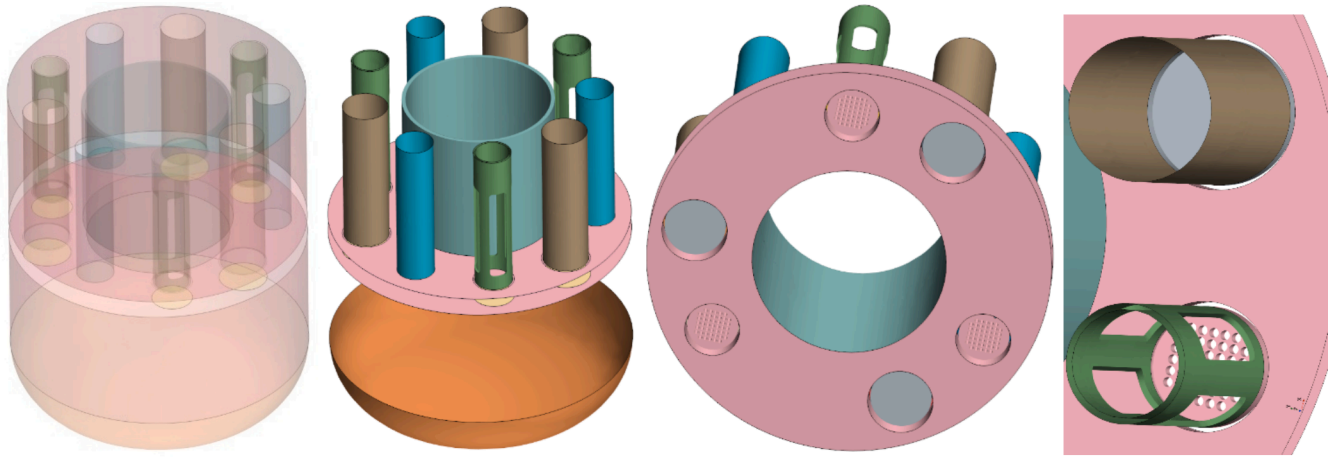

Fig. 7. Illustrations of the ALFRED mock-up geometry.

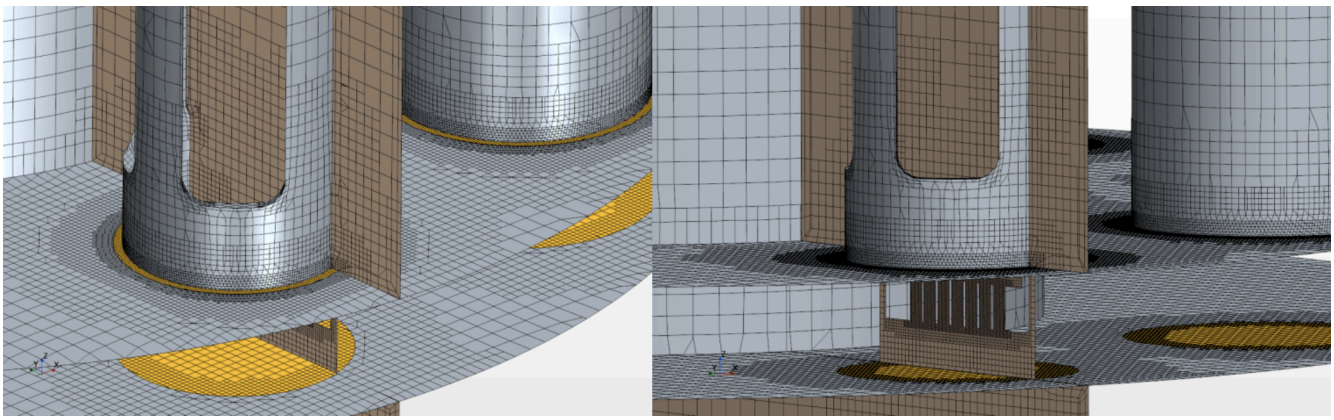

Fig. 8. ALFRED mock-up mesh illustration.

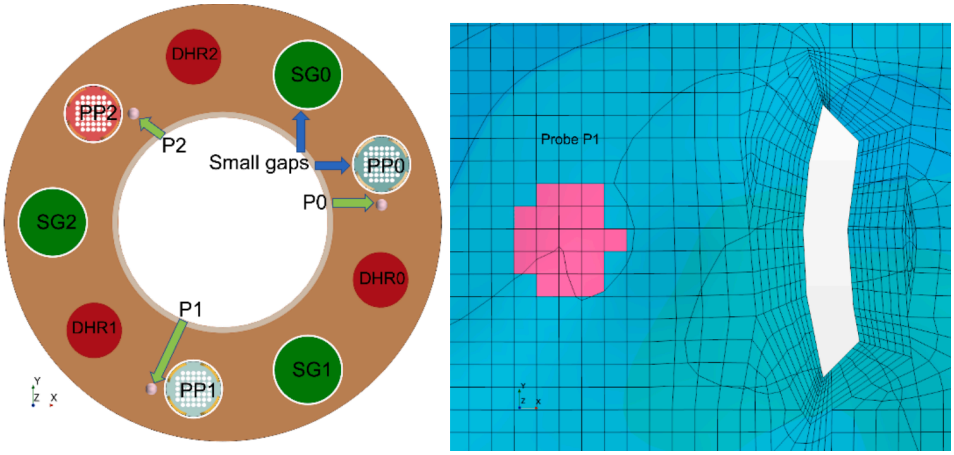

Fig. 9. Left, disposition of the components above the diaphragm. P0, P1 and P2 indicate the position of the capacitance probes. Right, domain of integration for the numerical probe P1 with an illustration of the mesh at the second level of adaptive refinement on the free-surface.

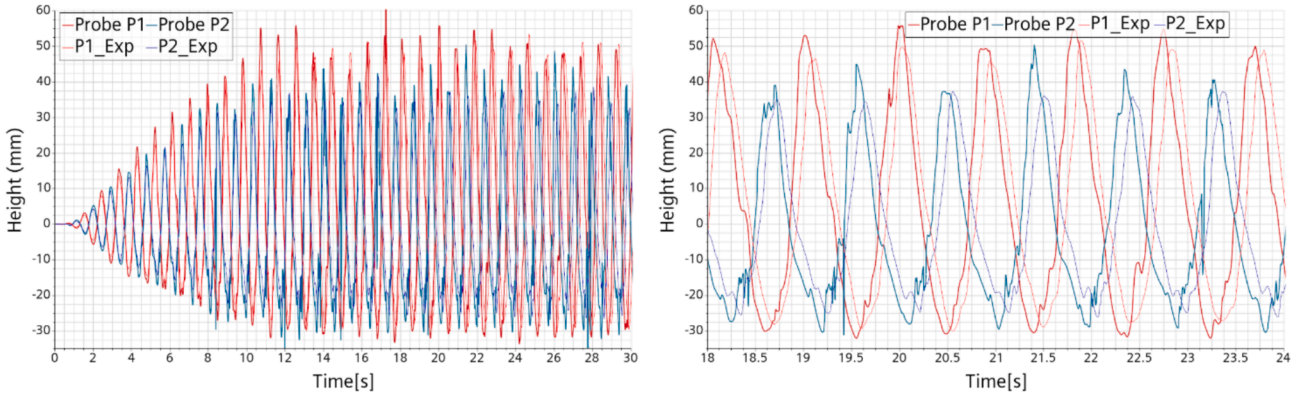

Fig. 10. Experimental/numerical comparison of the free-surface height under harmonic linear forcing amplitude 30 mm in direction Y at frequency 1.08 Hz. Height at 2 probes. Thicker numerical curves and corresponding thinner experimental curves. Left, interval 0–30 s. Right, zoom on interval 18–24 s.

require justification. However, now that we are concentrating our efforts on the forces acting on the structure, we could observe a five timesteps beat on the measured forces in coincidence with the periodic re-meshing. In our tests, the intensity of the force jump at re-meshing was of the same order as the local mean force and it was then reabsorbed during the next four timesteps. Being a very high frequency phenomenon, it has no observable effect on the flow. Switching back to the first order time scheme solved the issue, as shown in Fig. 12.

3.4. Earthquake simulations

In order to simulate a real earthquake, the scaling laws must be applied from the ALFRED design size to the mock-up size. The geometrical scaling ratio is about $1/18.4 = 0.0543$. Since the acceleration is an invariant of the scaling, the acceleration data can be used directly provided that time is consistently contracted. In other words, the flow of time for the mock-up is 4.29 faster than in the "real" world. The duration of an earthquake should be contracted accordingly. In

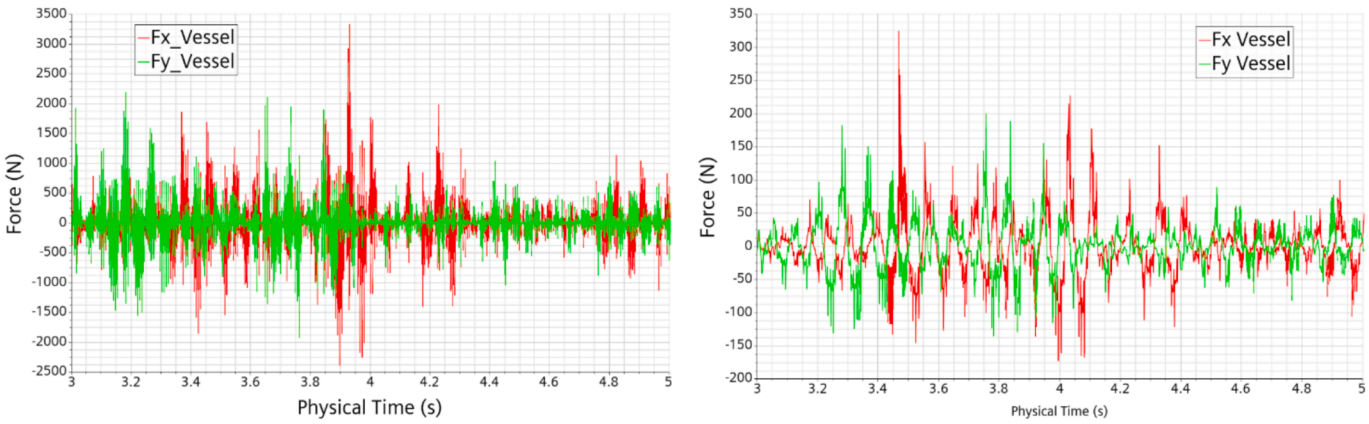

Fig. 11. Italian event. Forces on the vessel on a 3 s interval. Left: linear interpolation of the imposed displacement. Right: cubic interpolation.

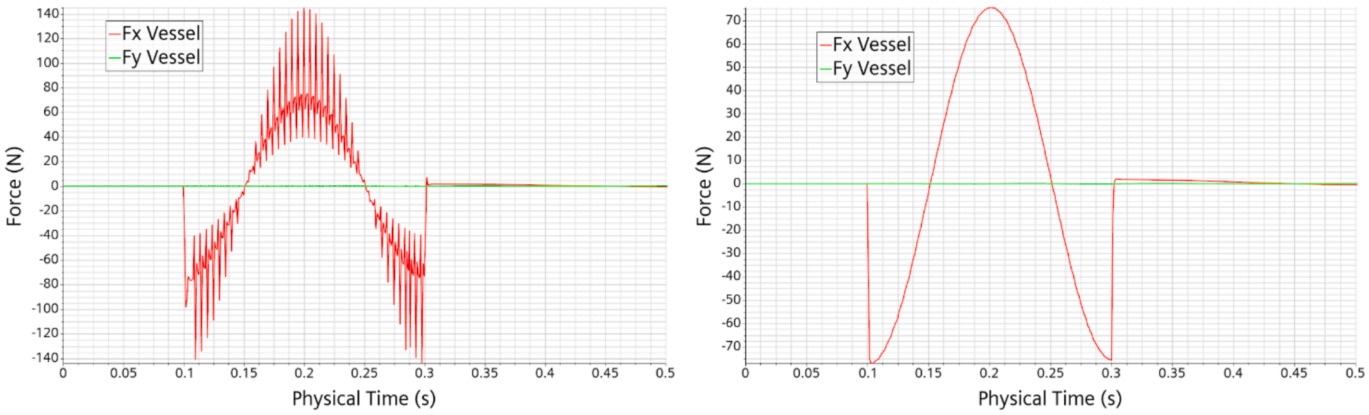

Fig. 12. Forces on the vessel under a 0.2 s harmonic pulse in direction X. Left, second order in time, Right, first order in time.

addition, the applied forces scale with the density and the volume of the fluid. In consequence, with a lead-water density ratio of 10.4, we have 1 N on the mock-up corresponding to about 10.4 * 18.4^3 = 65 kN on ALFRED.

In the following, the transposed effects on the ALFRED mock-up of four large seismic events of increasing magnitude are investigated. An animation of the mock-up displacement and its free-surface evolution can be downloaded here.[8]

3.5. Italian 2016 earthquake simulation

The earthquake, that occurred on October 30, 2016 near Perugia, caused the collapse of a huge number of buildings and the death of 299 people.[9] It is the earthquake of major magnitude, 6.5, found in the ISMD database (Luzi et al., 2020).

The displacement data table is downloaded from the ISMD database.[10] It is indicated that it is obtained from the processed acceleration: baseline correction and mean value removed, 4th order Butterworth filter applied with 0.1 Hz low cut and 45 Hz high cut frequency.

The displacement signal induced by the earthquake is shown in Fig. 13, left. The displacement applying the geometric and time scaling laws for the mock-up simulation is shown in Fig. 13, left. In front of the damage done, the displacement is surprisingly low and so is the free-surface height variation, as indicated in Fig. 14. However, the treatment of this event has allowed the procedure to be set up and the time scales involved to be understood.

3.6. Romanian 1977 earthquake simulation

The earthquake, which occurred on March 4, 1977, was estimated to have a magnitude of 7.5, although this was reduced to 6.3 at the site of acquisition. It caused the death of 1,578 people and destroyed or severely damaged about 32,900 buildings.[11]

This event is also the largest in Romania available in the ESM database.[12] Although relatively old, this earthquake is particularly significant because ALFRED is planned to be built in this country (Tarantino et al., 2021).

From the downloaded displacement table header, we can see that the baseline has been removed and a 2nd order Butterworth filter with a low-cut frequency of 0.2 Hz and a high-cut frequency of 25 Hz has been applied. The original source acceleration data is only recorded for 16.1 s. This translates into a 4 s shaking event for the mock-up. However, the maximum mock-up displacement reaches 1 cm, about 5 times the previous simulation, see Fig. 15, left. The free-surface elevation at the probes location is shown on Fig. 15, right, and reaches a maximum of 2 cm on probe P2.

The forces applied on the vessel are now sufficient to allow a clear interpretation. They can be related to the vessel acceleration. In Fig. 16,

[8] https://publications.crs4.it/pubdocs/2024/MP24a/.

[9] https://www.ansa.it/sito/notizie/speciali/2022/08/23/sei-anni-fa-il-terremoto-che-sconvolse-il-centro-italia_f2a36ead-529c-4f3a-bf3d-faebb2bfe77c.html.

[10] https://ismd.mi.ingv.it/evento.php?var1=8863681&path=161030064017&rev=man.

[11] https://en.wikipedia.org/wiki/1977_Vrancea_earthquake.

[12] https://esm-db.eu/#/event/RO-1977–0001.

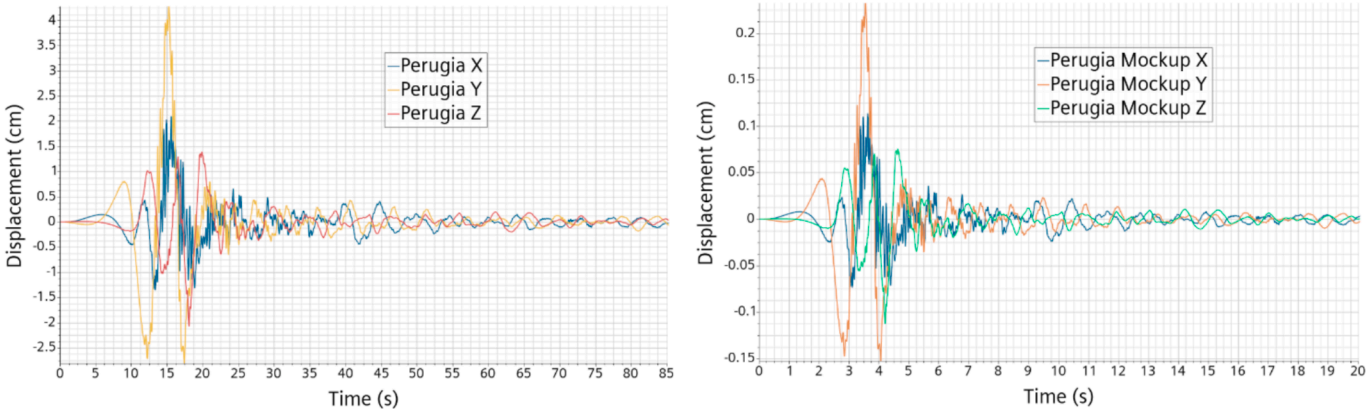

Fig. 13. Ground displacement in time for the Perugia event (left) and corresponding scale transposition for the ALFRED mock-up.

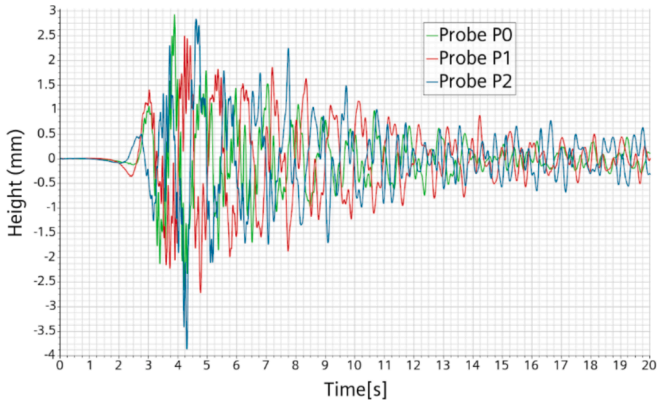

Fig. 14. Perugia event. Free-surface height at the probes in the ALFRED mock-up CFD simulation.

we provide a plot showing the acceleration and the force applied to the vessel in the Y direction. By adjusting the scales, we can make the two curves essentially coincide for the main part of the event during the first 5.5 s. Then, during the last 2.5 s, when the seismic acceleration has finished, there is a small residual oscillatory force at about 0.4 Hz which can be attributed to the sloshing.

The ratio of the force to the acceleration is given by the respective scales and gives about 33 kg. This value can be compared with the ~ 40 kg inventory of water.

3.7. Turkish 2023 earthquake simulation

In order to test our modelling with events of increasing magnitude, we now investigate the very recent large 2023 earthquake in Turkey. On February 6, 2023, the earthquake of magnitude 7.8 caused widespread damage over 350,000 km^2 and affected 14 million people of which 1.5 million were left homeless. The death toll for Turkey alone is 53,537 people.[13]

The data were measured at a distance of 24.6 km from the epicenter. Here again, the displacement data were taken from the ESM database used for the Romanian event. The baseline has already been removed and a 2nd order Butterworth filter with a low-cut frequency of 0.03 Hz and a high-cut frequency of 40 Hz high has already been applied. It can be seen that this filter is much weaker than the Romanian one, allowing larger displacement and stronger high frequencies. The displacement curve rescaled for the mock-up is shown on Fig. 17 left. The maximum horizontal displacement is now about 6 cm and comparable to the average 8.84 cm free-surface height above the diaphragm.

The free-surface elevation at the probes is given on Fig. 17 right. The magnitude of the elevation indicates a fairly strong free-surface agitation. The figure also indicates that for large displacement it is probably better to measure the free-surface height in a reference frame linked to the mock-up.

The three components of the acceleration applied to the mock-up are shown on Fig. 18 left. We can see that this seismic event lasts longer and is generally more intense than the Romanian one. The acceleration is shown together with the force on the vessel in direction Y on Fig. 18 right. Once again, we can see that the signals are strongly correlated with the “added mass” ratio which was found to be about 33 kg.

3.8. Japanese 2011 earthquake simulation

The largest earthquake ever recorded in Japan and the fourth largest worldwide since 1900, happened on March 11, 2011.[14] Of magnitude estimated to 9.0, with variations from 8.7 to 9.2, its epicenter was located about 72 km off the Pacific coast of the north-eastern region of Tohuku. The earthquake was followed by a deadly and devastating tsunami, which was also the triggering event for the infamous Fukushima accident. Combining the earthquake and the tsunami,”[t]he official figures released in 2021 reported 19,759 dead, 6,242 injured and 2,553 people missing.

The data comes from K-NET Tsukidate Miyaki prefecture site, about 50 km north-west of the Fukushima Daiishi Nuclear Power Plant (NPP). It has the highest recorded peak intensity, of about 2.8 g and the magnitude at the site is 6.6. It has been downloaded from the National Research Institute for Earth Science and Disaster Resilience (National Research Institute for Earth Science and Disaster Resilience, 2019).

The data consist of rough acceleration tables, without any filtering, for 300 s and sampled at 0.01 s. It is plotted on Fig. 19 in which we can observe that the peak is very high but also very sharp.

Displacement curves obtained from these data by successive integration would lead to completely inconsistent results, even after removing the baseline. Looking closely at the data, we observed a mean shift between the first ten seconds and the last ten seconds, indicating a likely shift in the sensors calibration during the most intense part of the earthquake. We divided the 300 s interval of the acceleration data in four segments, each with its own baseline correction. With these four degrees of freedom, we were able by trial and error, to impose zero displacement and slope at both the beginning and the end of the 300 s

[13] https://en.wikipedia.org/wiki/2023_Turkey%E2%80%93Syria_earthquakes.

[14] https://en.wikipedia.org/wiki/2011_T%C5%8Dhoku_earthquake_and_tsunami.

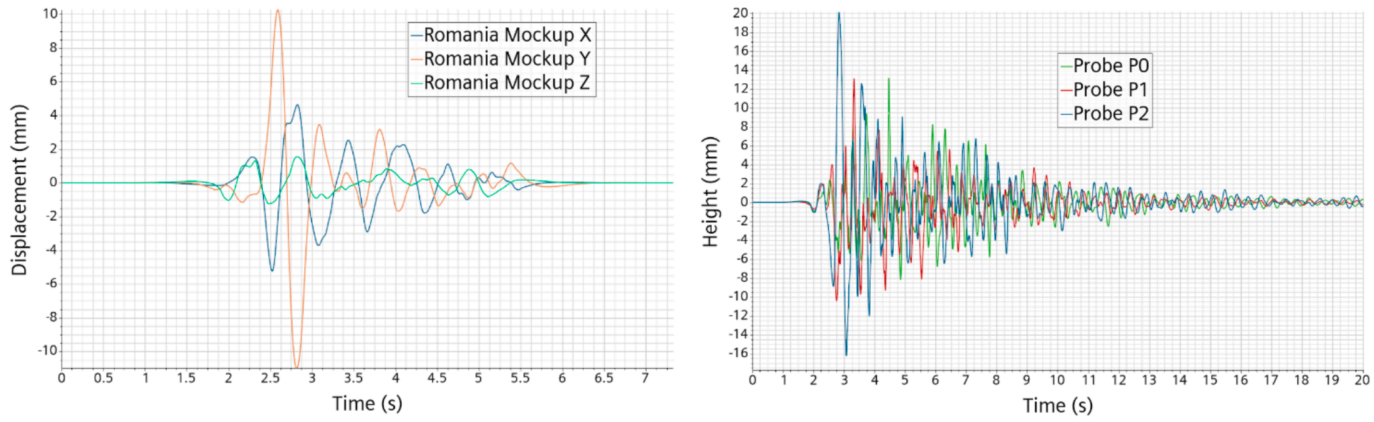

Fig. 15. Romania seismic event. Left, ALFRED mock-up displacement. Right, free-surface elevation at the probes.

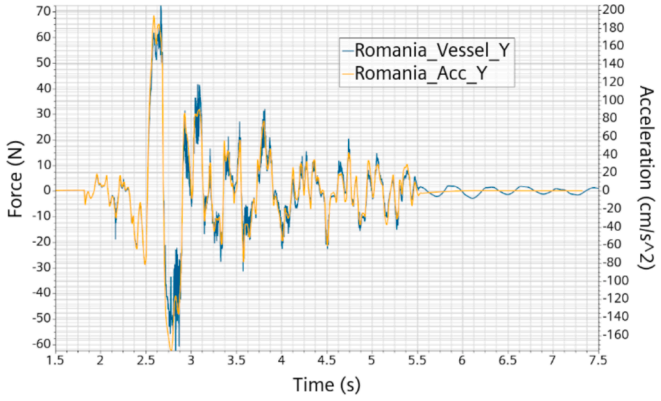

Fig. 16. Romania seismic event. Mock-up acceleration (orange) and force on the vessel (blue).

interval. It must be understood that a very small error in the acceleration induces a very large one in the displacement. In fact, an acceleration error of 1 mm/s^2 induces a displacement error of 45 m after 300 s. The arbitrariness of the method mainly lies in the choice of the four intervals. In retrospect, the imposition of a zero displacement at the end of the event is not consistent with (Miyazaki et al., 2011) which gives a final displacement about 1.5 m towards east. Also, a misunderstanding of the authors led us to set the vertical direction upward whereas the data and, more generally, the seismology community makes it in the (UD, Up-Down) gravity direction. Thus, all the simulated displacements are only representative of the intensity and duration of the events, which is all that is needed in the context of this paper.

The displacement on site is given in Fig. 20. It exceeds 3 m in direction X. Applied to the mock-up, it is more than 18 cm, that is more than twice the allowed range in SHAKESPEARE. To illustrate this point, in Fig. 21, we show the mock-up at start and at maximum displacement after 22 s, the two plots being taken from the same point of view.

The sloshing is quite limited with a maximum of 16 mm of elevation at the probes, in the mock-up reference frame. Consistently with the Turkey seismic event, the ratio of the force on the vessel to the acceleration is also found to be in the range 32.6–32.9 kg.

3.9. *Japanese 2011 earthquake simulation with damped mock-up*

The previous Japan 2011 earthquake simulation was performed using raw data, in which high frequencies were limited only by the sampling frequency at 100 Hz. The stepwise removal of the baseload had no effect on the high frequencies. The forces applied to the vessel correlate very precisely with the imposed acceleration. A reactor such as ALFRED should have a damping system, to absorb the high frequencies. We have no information about this damping system but our first guess is that it should work in a similar way to a low-pass filter. So, we apply a Butterworth 1 Hz low-pass filter to the acceleration data over the full 300 s time-scale and then proceed to generate the new mock-up displacement data.

The maximum difference between the displacement curves of the mock-up is 8.6 mm in direction X. On site, this would be 15.8 cm, which could be interpreted as the required deformation of the damping system. In terms of instantaneous acceleration, the filter has an enormous effect. As shown on Fig. 22, the acceleration magnitude is lower by one order of magnitude. But looking at the flow elevation at the probe in Fig. 23, the global difference in intensity with the unfiltered case is only marginal.

The acceleration still correlates very well with the force applied to the vessel, see Fig. 22, right. When the acceleration decreases towards the end of the simulation, it becomes clearer that there is also a small but observable other contribution to the force. We ascribe this contribution to the sloshing effect. A residual sloshing of about 2 mm amplitude can be observed at the end of the simulation, as shown on Fig. 23.

4. Summary and discussion

The material presented here summarizes four years of activity in the framework of the PASCAL project with the aim “To further enhance the modelling and computational readiness level of sloshing dynamics in compact liquid–metal filled pools and to retrieve the expected impact forces and dislocations on the involved components for a reference system (e.g. ALFRED).”

While it is nowadays relatively easy and straightforward to simulate sloshing qualitatively with CFD, taking the simulation to quantitative validation is much more demanding. It is not surprising a posteriori that we could not find such a validation for the simple case of a partially filled vertical cylinder subject to a harmonic oscillation. However, we did find the very well documented and comprehensive experimental work by Royon-Lebeaud (Royon-Lebeaud, 2005; Hopfinger and Baumbach, 2009), which became the backbone of our analysis. Having in mind an extrapolation to ALFRED under seismic events, it was also natural to study a larger cylinder and focus on the initial evolution of the sloshing wave rather than only on its asymptotic amplitude.

It turns out, rather unexpectedly, that the effect of the cylinder radius on the dimensionless frequency-amplitude map is far from negligible. This was first discovered experimentally at VKI, and then confirmed numerically at CRS4. It should be emphasized that without the experimental data provided by VKI, the CRS4 results would not have been publishable as they were obviously apparently inconsistent with the existing literature. Alternatively, it would have been erroneously concluded that CFD simulations cannot correctly predict the transition to chaos. This is to justify the practice, now consolidated in the HLM Gen-IV community of combining experimental campaigns with

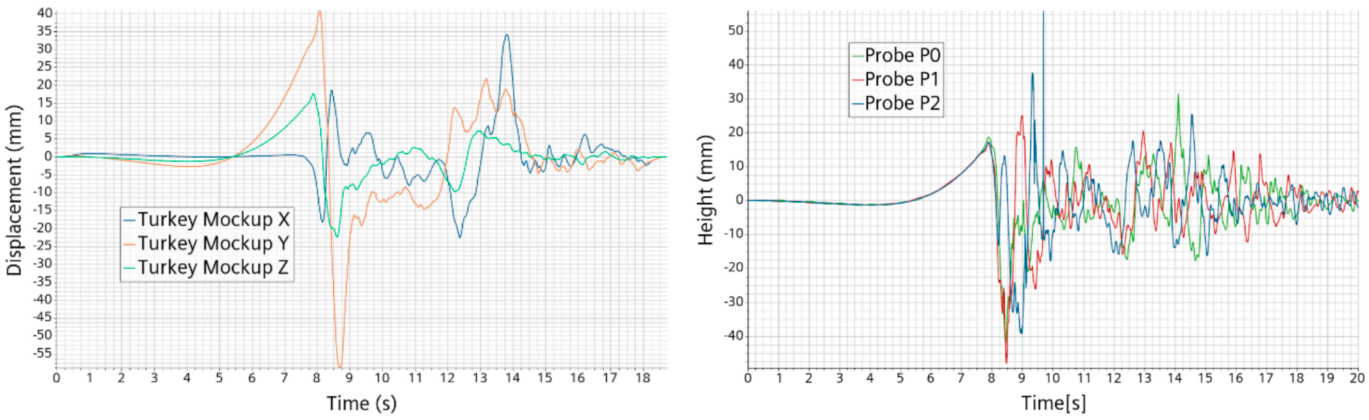

Fig. 17. Turkish seismic event. Left, ALFRED mock-up displacement. Right, free-surface elevation at the probes.

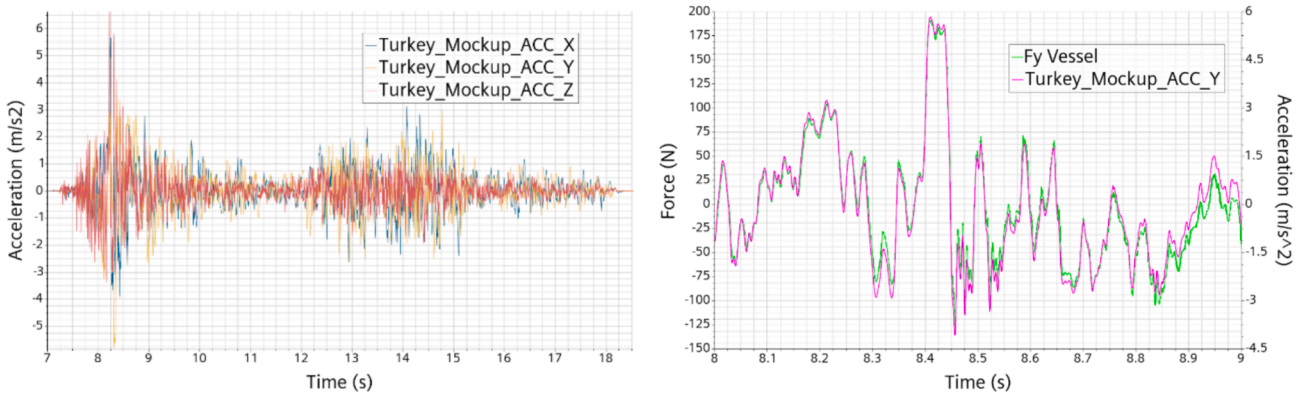

Fig. 18. Turkish seismic event. Mockup imposed acceleration (left). Comparison force on the vessel vs. acceleration around the peak acceleration (right).

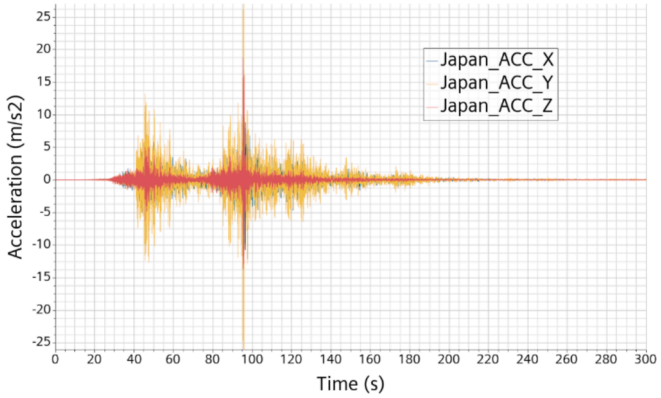

Fig. 19. Japan seismic event. Acceleration from the database.

numerical simulation, ultimately allowing a cross-validation of the results.

The validation of the numerical model is not only based on the correct value of the transition to chaotic behavior but also, and above all, on the correct reproduction of the initial evolution of the wave, which includes the low frequency modulation and its evolution while approaching the critical value. Moreover, all the phases of the flow within the chaotic region are also clearly identified. This is not only a validation of the numerical model, but it is also a strong validation of the underlying theoretical model within the VoF framework and the ability of its implementation in the software to represent complex flows.

The validation, however, was focused on the free-surface position and its time evolution, i.e. on velocity. The impact of forces on the vessel or the components requires a higher order of validation, as Newton's law requires the acceleration to be tightly controlled. It turns out that for seismic events, acceleration peaks come from the highest frequencies represented. Therefore, these high frequencies must be correctly taken into account in the numerical model.

With regard to the preliminary treatment of the seismic data, we need to look carefully at several relevant features:

- The tabular form of the input displacement data is sampled at 0.01 s intervals, which practically cuts off the frequencies above 100 Hz.
- The simulation time-step, CFL- controlled, coincidentally much lower than the sampling interval.
- The data of the first three earthquakes were regularized with a high frequency cut between 25 to 40 Hz.
- In addition, the low frequency cut in fact forces the final position to be the same as the initial position.
- Spurious acceleration peaks are induced by the displacement data linear interpolation. This results in spurious peaks in the measured forces. Decreasing the time-step worsen the situation.
- Cubic interpolation of the displacement data removes the spurious acceleration peaks. In practice, it reproduces a high frequency cut.

Moreover, there is a specific issue with the interaction of the second order temporal scheme with the adaptive meshing. The interaction works perfectly as far as the velocity field is concerned but introduces a high frequency pressure beat coinciding with the 5 time-steps re-meshing interval. The high frequency pressure beat is directly translated into a force pulsation on the structures. Its intensity is of the same order as the force averaged over 5 time-steps. This pulsation combines with the pulsation resulting from the interpolation of the displacement data

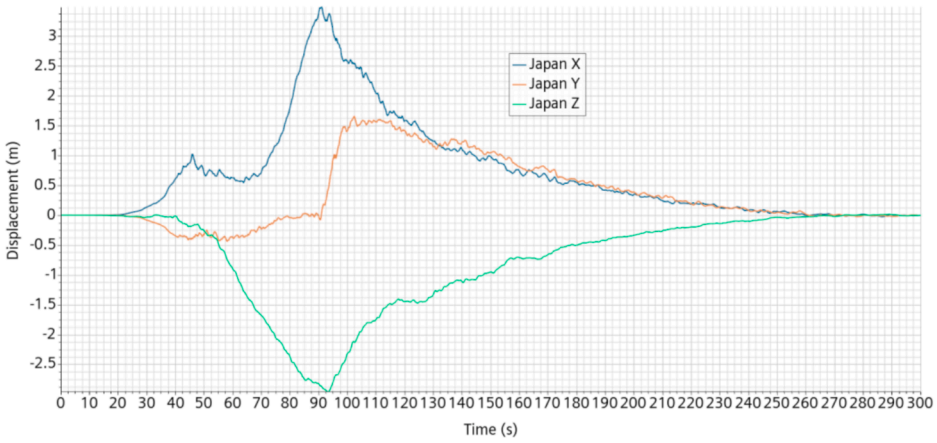

Fig. 20. Japan seismic event. On site reconstructed displacement.

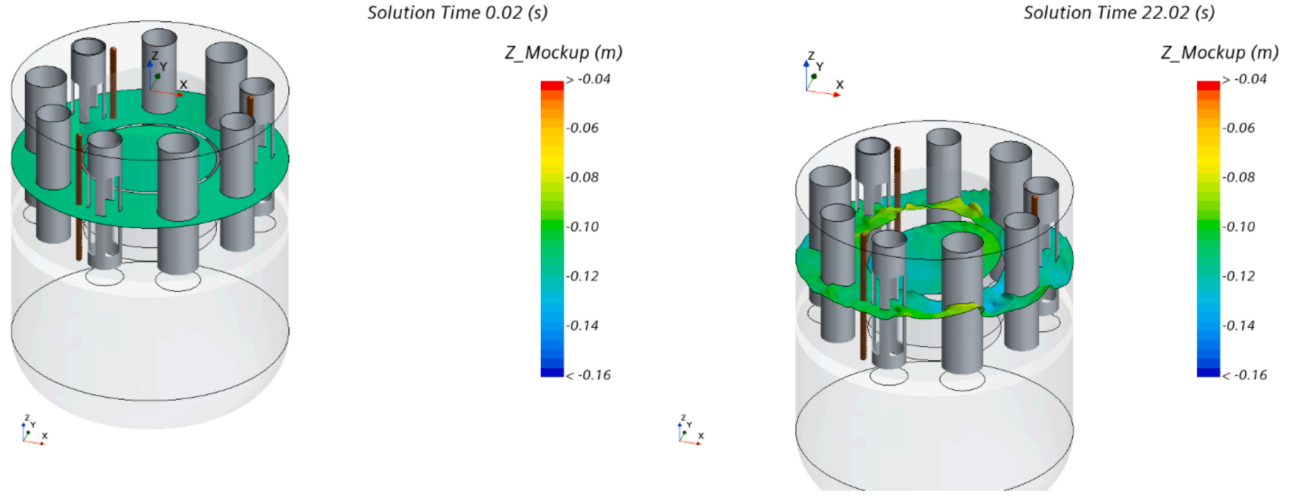

Fig. 21. Japan seismic event. Relative position in a fixed frame of the mock-up at start and after 22 s.

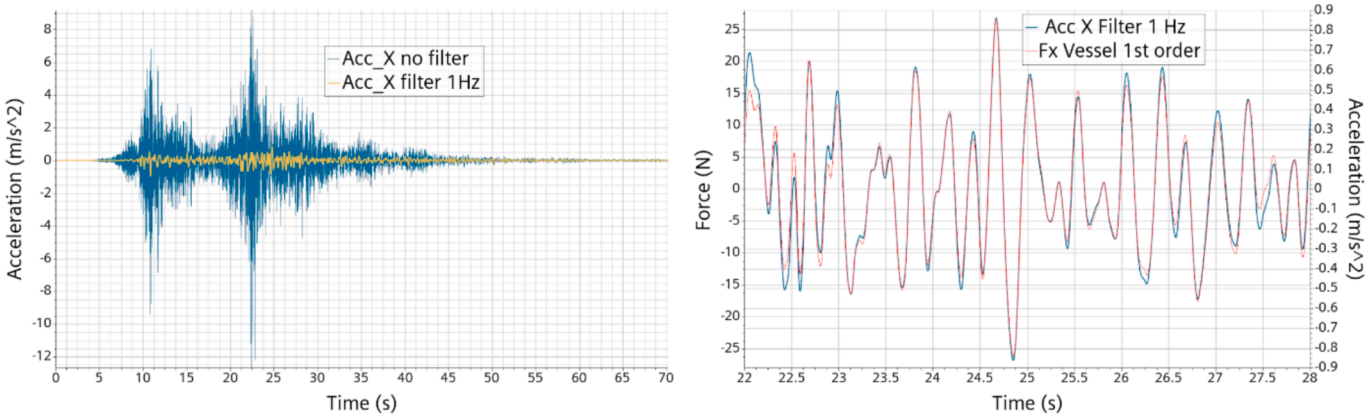

Fig. 22. Japan seismic event. Left, effect of the 1 Hz low pass filter on the acceleration. Right, 1 Hz filtered simulation. Force on the vessel vs. acceleration during the event peak intensity.

making it difficult to detect at first. Switching back to the first order in time numerical scheme effectively solves the problem.

The hopefully complete numerical control of the spurious acceleration-induced force peaks was only achieved at a very late stage of the project. The cleaned force signal is strongly correlated to the imposed seismic acceleration, with only a tiny contribution coming from the surface wave. It is therefore clear that an "unprotected" ALFRED is much less threatened by sloshing effects during a severe seismic event than by the high frequency vibrations which are way more soliciting.

Obviously, there is no such thing like an "unprotected" ALFRED, and ALFRED must be protected by a damping system. Without any knowledge of such a system, we assume that its effect is similar to applying a

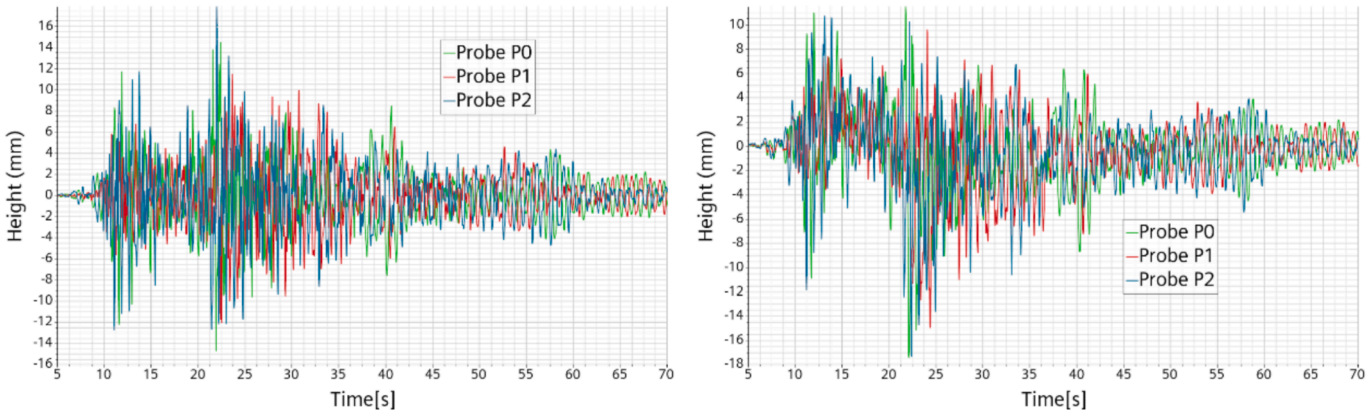

Fig. 23. Japan seismic event. Free-surface numerical height at the probes. Left, unfiltered displacement. Right, low pass filter at 1 Hz applied.

low-pass filter to the input forcing data. We applied this idea to the Japan event with a Butterworth 1 Hz low pass filter. The effect is the reduction of the forces by one order of magnitude. The effect on the displacement is however very limited with a maximum variation on the mock-up about 8.6 mm, which is equivalent to 15.8 cm on site. This variation is what the damping system should be able to withstand. Under these new conditions, the forces are still strongly correlated to the acceleration. The sloshing effect remains small during the most critical part of the event but survives and becomes dominant towards the end of the event. It never really becomes significant.

For the seismic events studied, the mock-up behavior is very similar to that of a forced solid displacement with the vessel withstanding about 31–33 kg of water "added mass" and the remaining 7–9 kg being split between the components and mostly the inner circular wall.

5. Conclusion

As requested, this work improves the modelling and computational readiness level of sloshing dynamics in compact liquid–metal filled pools and shows that it is possible to retrieve the expected impact forces on the components involved. Specifically, it shows that CFD simulations can be made quantitatively accurate enough to capture a stability transition behavior very accurately.

While surely not optimal on the timing, the applied methodology combines a strong interaction with the experimental side of the activity while still leaving room for a certain level of serendipity. In short, simulations have very small value without experimental confirmation, but once this is acquired, extrapolation to situations not experimentally reachable can be performed with a reasonable confidence in the results.

Beyond the CFD model validation, by applying the modelling to significant seismic events, we observed that the dominant impact forces are related to the highest withstood frequencies. While concerns about sloshing effects remain legitimate, a much greater concern should be the importance of protecting ALFRED with a carefully designed damping system.

CRediT authorship contribution statement

Vincent Moreau: Writing – review & editing, Writing – original draft, Visualization, Validation, Methodology, Data curation, Conceptualization. **Manuela Profir:** Writing – review & editing, Writing – original draft, Visualization, Validation, Methodology, Data curation, Conceptualization.

Funding

This work has received funding from the Euratom Research and Training Programme 2019–2020 under the Grant Agreement No 945,341 (PASCAL).

Declaration of competing interest

The authors declare that they have no known competing financial interests or personal relationships that could have appeared to influence the work reported in this paper.

Acknowledgments

The authors want to thanks G. Siddi-Moreau for writing the software used to apply the filters to the data and for the accurate review.

Data availability

Data will be made available on request.

References

Cioli Puviani, P., Di Piazza, I., Marinari, R., Zanino, R., Tarantino, M., 2024. Multiscale thermal-hydraulic analysis of the ATHENA core simulator. Nucl. Technol. 210 (4), 692–712. https://doi.org/10.1080/00295450.2023.2215682.

Frandsen, J., Grasso, V., Muller, J., Cantiani, A., Laboureur, D., Koloszar, L., Planquart, P., 2024. Results of the experimental campaign with SHAKESPEARE, PASCAL EURATOM project 945341, deliverable D22, (submitted).

Grasso, V., 2024. Experimental investigation of sloshing on the Advanced Lead Fast Reactor European Demonstrator, Master thesis. Politecnico Di Torino. http://webthesis.biblio.polito.it/id/eprint/31200.

Hopfinger, E.J., Baumbach, V., 2009. Liquid sloshing in cylindrical fuel tanks. Prog. Propulsion Phys. 1, 279–292. https://doi.org/10.1051/eucass/200901279.

Luzi, L., Lanzano, G., Felicetta, C., D'Amico, M., C., Russo, E., Sgobba, S., Pacor, F., & ORFEUS Working Group 5, 2020. Engineering Strong Motion Database (ESM) (Version 2.0). Istituto Nazionale di Geofisica e Vulcanologia (INGV). https://doi.org/10.13127/ESM.2.

Miyazaki, Shin'ichi, McGuire, Jeffery J., Segall, Paul, 2011. Seismic and aseismic fault slip before and during the 2011 off the Pacific coast of Tohoku Earthquake. Earth Planets Space 63 (637–642). https://doi.org/10.5047/eps.2011.07.001.

Moreau, V., Profir, M., CFD modeling and validation of a GEN-IV reactor mockup under seismic load, PASCAL EURATOM project 945341, deliverable D38, 2024 (submitted) https://publications.crs4.it/pubdocs/2024/MP24d.

Moreau, V., Profir, M., Sloshing CFD modeling and validation with SHAKESPEARE first experimental campaign, PASCAL project deliverable D13, 2023 https://cordis.europa.eu/project/id/945341/results.

Moreau, V., Profir, M., Keijers, S., Van Tichelen, K., 2019. An improved CFD model for a MYRRHA based primary coolant loop. Nucl. Eng. Des. 353, 110221.

Muller, J., Planquart, P., Laboureur, D., 2023. Experimental investigation of the transition between linear to chaotic regimes of sloshing. Multiphase Sci. Technol. 35 (4), 63–74. https://doi.org/10.1615/MultScienTechn.2023047903.

Myrillas, K., Planquart, P., Buchlin, J.-M., Schyns, M., 2015. CFD and experimental investigation of sloshing parameters for the safety assessment of HLM reactors, NURETH-16, Chicago, NURETH-16, Chicago, IL, August 30-September 4.

National Research Institute for Earth Science and Disaster Resilience, 2019. NIED K-NET, National Research Institute for Earth Science and Disaster Resilience, doi:10.17598/NIED.0004.

Royon-Lebeaud, A., 2005. Ballottement des liquides dans les réservoirs cylindriques soumis à une oscillation harmonique: régimes d'onde non-linéaire et brisure.

Mécanique [physics.med-ph]. Université Joseph-Fourier - Grenoble I. Français. tel-00009117.

Sharma, V., Arun, C.O., Praveen Krishna, I.R., 2019. Development and validation of a simple two degree of freedom model for predicting maximum fundamental sloshing mode wave height in a cylindrical tank. J. Sound Vibration 461 114906. https://doi.org/10.1016/j.jsv.2019.114906.

Tarantino, M., Angiolini, M., Bassini, S., Cataldo, S., Ciantelli, C., Cristalli, C., Del Nevo, A., Di Piazza, I., Diamanti, D., Eboli, M., et al., 2021. Overview on lead-cooled fast reactor design and related technologies development in ENEA. Energies 14, 5157. https://doi.org/10.3390/en14165157.